European Journal of Mechanics / A Solids 96 (2022) 104748

Contents lists available at ScienceDirect

European Journal of Mechanics / A Solids

journal homepage: www.elsevier.com/locate/ejmsol

A novel discrete coordinate approach to modelling nonlinear structural instability problems with material damage

Anton Köllner [a,b,*], M. Ahmer Wadee [a]

[a] Department of Civil and Environmental Engineering, Imperial College London, London SW7 2AZ, United Kingdom
[b] Institute of Mechanics, Stability and Failure of Functionally Optimized Structures Group, Technische Universität Berlin, Einsteinufer 5, 10587 Berlin, Germany

ARTICLE INFO

Keywords:
Structural instability
Damage
Buckling
Composite structures
Delamination
BVID

ABSTRACT

A novel analytical framework for the inclusion of active damaging processes in a structural stability analysis is presented. The framework considers quasi-static deformation processes and is formulated in terms of a discrete coordinate approach, employing an extended total potential energy functional, where the current damage state is expressed in terms of geometric configuration and applied loading. Within the current framework, an efficient analysis of structures prone to buckling instability and material damage is enabled particularly where damage initiates once structural instability has been triggered. Composite panels with multiple damage mechanisms (*e.g.* delaminations, matrix cracks) are studied to showcase its application.

1. Introduction

The failure of structures is characterized by a more or less sudden loss in load carrying capability. This concept applies to both material and structural failure. In the former, changes in the material (*e.g.* damage and/or plastic accumulation or fracture) trigger instability while in the latter the geometry is, or becomes, unsuitable that results in structural instability (buckling).

The loss of structural stability in a mechanical system can constitute a catastrophic failure scenario. This type of failure is strongly related to slender structures, which can be found in a vast variety of applications principally in the transportation and construction industries. The exposition presented herein focuses on such structures for which buckling instability must be accounted when evaluating the structural behaviour.

Nevertheless, material damage may also influence global structural stability. This is of particular interest for structures made from composite materials, *e.g.* multi-layered fibre reinforced polymer laminates that are vulnerable to various damage mechanisms, for instance matrix cracking and delamination growth; however, this also applies to more traditional construction materials (*e.g.* structural steel) where plastic deformations and/or micro-cracking may occur during post-buckling deformation.

Well-established general theories of structural stability consider elastic systems and may be regarded as a reasonably mature subject (Thompson and Hunt, 1973; Bažant and Cedolin, 2010; Koiter, 1945). Stability of deformation states are conveniently evaluated by analysing the total potential energy of the system. The change in total potential energy with respect to small perturbations is studied by means of variational calculus. This applies to both the discrete coordinate approach (Thompson and Hunt, 1973) and the continuous description (Koiter, 1945). To date, structural stability theories that consider the effect of damage and its growth are practically non-existent. This constitutes a significant gap within structural stability analysis techniques and the presented work aims for this to be filled.

In solid mechanics, conditions for the (in)stability of time-independent elastic–plastic (inelastic) media (Hill, 1958, 1962; Petryk, 1991) are derived based on variational (extremum) principles. The solution of the underlying general boundary value problem, in terms of velocity fields, where time is not necessarily understood to be natural time, assigns a stationary value to a functional comprising a constitutive potential and loading associated potentials expressed in terms of rates of (nominal) surface tractions and rates of body forces (Hill, 1958). A fundamental quasi-static deformation process is stable whenever the solution is also a minimizer of the functional (Petryk, 1991, 2005). In the context of fracture, deformation paths and their stability are determined by defining the total energy comprising an elastic part and a dissipative part associated with, for instance, crack propagation (Del Piero, 2013; Francfort and Marigo, 1998). The deformation path is obtained by a variational principle perturbing the configuration and the damage state, where an equilibrium configuration makes the governing functional to be non-negative alongside compliance with the second law of thermodynamics (as part of the Kuhn–Tucker conditions

* Corresponding author at: Institute of Mechanics, Stability and Failure of Functionally Optimized Structures Group, Technische Universität Berlin, Einsteinufer 5, 10587 Berlin, Germany.
E-mail address: anton.koellner@tu-berlin.de (A. Köllner).

https://doi.org/10.1016/j.euromechsol.2022.104748
Received 24 November 2021; Received in revised form 21 June 2022; Accepted 22 July 2022
Available online 27 July 2022
0997-7538/© 2022 The Authors. Published by Elsevier Masson SAS. This is an open access article under the CC BY license (http://creativecommons.org/licenses/by/4.0/).

for variational problems with unilateral constraints), *i.e.* healing is not permitted (Maugin, 1999). The concept can also be extended to cohesive (ductile) fracturing processes (Del Piero, 2013).

In contrast with the current work, in which focus is placed on deformation processes where structural instability is deemed to occur before inelastic deformation is caused (see below for characteristic application examples), the aforementioned studies focused on the stability of solids undergoing inelastic deformation. This is of particular relevance for problems where inelasticity is present before structural instability occurs, *e.g.* plastic buckling (Hutchinson, 1974; Tvergaard, 1983; Petryk and Thermann, 1992), or inelastic deformation is the source of instability (material instability), *e.g.* necking, shear bands (Bigoni, 2000; Bordignon et al., 2015) and unstable crack propagation (Bourdin et al., 2008; Sumi et al., 1985).

In order to enable an efficient description of inelastic deformation, a work potential theory (Schapery, 1987, 1990), also referred to as Schapery theory, has been presented which employs the assumption of path independence during damaging processes (at least in a limited sense). It is demonstrated that for stable processes, a work-like potential can be derived so that deformations exhibiting a change in structure (*e.g.* damage and/or plasticity) can be described by generalized displacements only. Although the work does not attempt to provide a general description of damage as in Del Piero (2013) and Francfort and Marigo (1998), it does provide an efficient method to describe deformations exhibiting stable damage propagation.

In the context of structural stability, a formalism that is capable of considering inelastic deformation once buckling instability has occurred appears to be missing. The increasing use of composite materials in lightweight (slender) structures and challenges regarding improved sustainability, *i.e.* in the present context this means utilizing the full potential of engineering structures, highlights the need for such a formalism. For instance, damage tolerant design is a requirement in the aircraft industry (Nettles and Douglas, 2000; European Union Aviation Safety Agency (EASA), 2019; Köllner et al., 2021), which demands the consideration of damage within the design process. Hence, structures vulnerable to buckling instability must be analysed considering inelastic deformation and its effect on the load-carrying capacity. Standard tests evaluating the strength of damaged composite structures are termed 'compression-after-impact' or 'tension-after-impact' loading scenarios (Tan et al., 2016; Sun and Hallett, 2018; Liu et al., 2017). Various damage mechanisms such as delaminations, matrix cracks and fibre breakage may affect the global stability of such composite panels (Köllner et al., 2020; Köllner and Völlmecke, 2018; Calvo et al., 2022; Wang et al., 2020; Juhász and Szekrényes, 2015, 2017), which also applies to sandwich panels (Wadee and Blackmore, 2001; Wadee, 2002). Furthermore, regarding structural members in civil engineering applications, ultimate strength predictions, as used in design codes, may involve plastic deformation and micro-cracking during the post-buckling response (Abambres et al., 2014; Gardner, 2008, 2019; Gonçalves and Camotim, 2012; Bai et al., 2021).

The current framework enables an efficient stability analysis of such structures, *i.e.* slender engineering structures prone to buckling instability and material damage. Therefore, a discrete coordinate approach is employed, so that semi-analytical models of structural members subjected to compressive loading can be developed. As a consequence, the instability behaviour of such mechanical systems can be systematically and efficiently explored, thus allowing a better understanding of the mechanical responses. As aforementioned, problems exhibiting buckling instability during inelastic deformation (*e.g.* plastic buckling) are not within the scope of the current work. The analytical framework employs an extended total potential energy functional comprising reversible and dissipative energy contributions, where with the aid of the concept described in Schapery (1990), the damage state – whenever inelastic deformation is present – is expressed in terms of the current structural configuration and the applied loading. Thus, the novel framework enables the consideration of inactive and active damage mechanisms within a structural stability analysis.

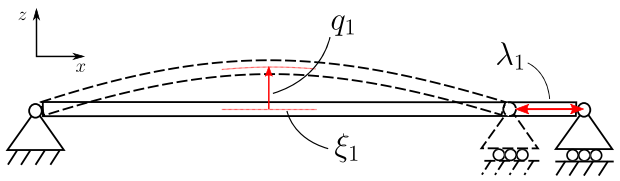


Fig. 1. Euler strut; generalized coordinate q_1 – amplitude of buckling displacement, load parameter λ_1 – end-shortening, damage parameter ξ_1 – delamination length/area.

In the subsequent exposition, the underlying theoretical concept is described in Section 2. The analytical framework is provided in Section 3. In Section 4, the theory is applied to the problem of a composite plate strip with multiple damage mechanisms. Capabilities and limitations of the novel framework are discussed in Section 5 with conclusions being drawn in Section 6.

2. Underlying concept

The present framework considers mechanical systems that can be described by sets of generalized coordinates q_i ($i = \{1, 2, \dots, I\}$), loading parameters λ_m ($m = \{1, 2, \dots, M\}$) and damage parameters ξ_k ($k = \{1, 2, \dots, K\}$). The parameters are exemplarily visualized by means of a standard Euler strut in Fig. 1. For the simple example shown, the geometric configuration is represented by the amplitude (generalized coordinate q_1), the load parameter is, in effect, defined by the applied end-shortening, while the damage parameter could be a delamination length/area or a micro crack density. In general, damage parameters may be geometric representations of defects and damage such as (micro) crack densities and delamination areas, physical quantities such as strain measures (*e.g.* plastic strain) or even dissipative energies associated with respective damage mechanisms.

With the aid of characteristic deformation processes shown in Fig. 2, a relationship between damage propagation and stability is established next. In Figs. 2(a) and 2(b), the well-known double cantilever beam (DCB) test and the corresponding force (P) versus displacement (u) behaviour are illustrated respectively. The initial delamination length is denoted by ξ. The mechanical response comprises two parts. First, the beam deforms elastically (black line in Fig. 2(b)), thus there is no change in structure, *i.e.* no delamination growth ($\dot{\xi} = 0$), with the energy release rate (ERR) being smaller than its respective critical threshold ($G < G_c$). At the deformation state denoted by (u^0, P^0), the ERR reaches the critical ERR ($G = G_c$) and delamination growth is initiated. It should be noted that under force-controlled loading (dead loading), the beam would fail under unstable delamination growth at (u^0, P^0). However, in a displacement-controlled configuration (rigid loading), the red path in Fig. 2(b) highlights the actual deformation path under quasi-static loading, where the delamination grows from one load step to another ($\dot{\xi} > 0$) and equality between the ERR and its critical threshold holds throughout the deformation path ($G = G_c$). Hence, under displacement-controlled loading stable delamination growth is present, *i.e.* for a constant state of loading delamination growth stops.

Stable damage propagation under displacement-controlled loading can also be observed for matrix crack growth in composite laminates, where Figs. 2(c) and 2(d) illustrate a buckled strut with matrix cracks and the associated damage growth behaviour respectively. The matrix cracks are defined in the form of a matrix crack density D_{mc} (*cf.* Köllner et al., 2020; Kashtalyan and Soutis, 2000) and Fig. 2(d) shows the behaviour of the ERR for matrix crack growth against the matrix crack density ($\xi = D_{mc}$) for increasing levels of load input (applied displacement/end-shortening $\lambda = \mathcal{E}$), *i.e.* $\lambda^{I} < \lambda^{II} < \lambda^{III}$. The monotonically falling ERR with increasing crack density for a constant state of loading underlines the behaviour described for the DCB test,

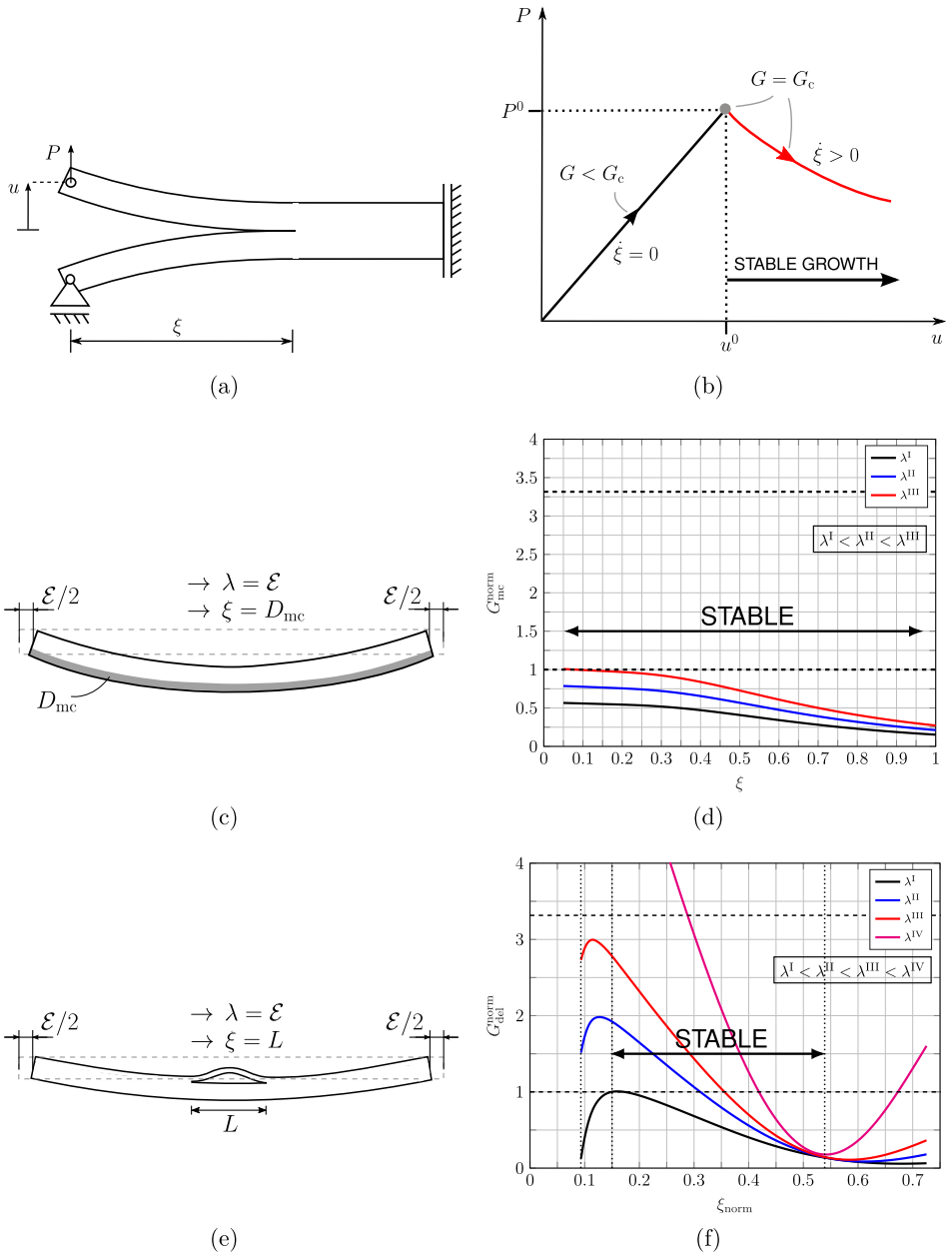


Fig. 2. Characteristic deformation processes; (a)–(b) DCB test and its force P vs. displacement u behaviour; (c)–(d) Matrix crack growth during buckling (bending deformation) and its corresponding behaviour of the ERR $G_{\mathrm{mc}}^{\mathrm{norm}}$ vs. matrix crack density D_{mc} for increasing load input λ; (e)–(f) Delamination buckling and its corresponding behaviour of the ERR $G_{\mathrm{del}}^{\mathrm{norm}}$ vs. delamination length L for increasing load input λ; stable regions highlighted whenever $\mathrm{d}G/\mathrm{d}\xi\big|_{\lambda} < 0$. (For interpretation of the references to colour in this figure legend, the reader is referred to the web version of this article.)
Source: (c)–(f) adapted from Köllner et al. (2020)

where damage propagation stops under constant loading characterizing stable damage growth behaviour, thus $\mathrm{d}G/\mathrm{d}\xi\big|_{\lambda} < 0$. As a consequence, in the loading process (displacement-controlled), throughout matrix crack growth, the equality $G = G_{\mathrm{c}}$ holds, which indicates a stable damaging process such that the loading (during damage growth) follows the horizontal line represented by $G_{\mathrm{mc}}^{\mathrm{norm}} = G/G_{\mathrm{c}} = 1$ in Fig. 2(d).

The same analysis can be applied to the well-known problem of delamination buckling (*cf.* Köllner et al., 2020; Köllner, 2021) visualized in Fig. 2(e), where the damage parameter is the delamination length ($\xi = L$). Fig. 2(f) shows the behaviour of the ERR for delamination growth against the delamination length for increasing levels of load input with $\lambda^{\mathrm{I}} < \lambda^{\mathrm{II}} < \lambda^{\mathrm{III}} < \lambda^{\mathrm{IV}}$ ($\lambda = \mathcal{E}$). As for matrix crack growth, a region of stable delamination growth can be identified in Fig. 2(f), where $\mathrm{d}G/\mathrm{d}\xi\big|_{\lambda} < 0$ and growth is governed by the equality $G = G_{\mathrm{c}}$, *cf.* $G_{\mathrm{del}}^{\mathrm{norm}} = 1$ in Fig. 2(f). Note that a monotonically falling ERR illustrates that for a constant state of loading delamination growth stops and further loading may be applied. A comprehensive analysis of the damage growth behaviour in composite laminates undergoing buckling deformation can be found in Köllner et al. (2020).

In conclusion, it has been shown that for quasi-static deformation processes exhibiting stable damage growth equality holds between the physical quantity available to produce a change in structure (*e.g.* the ERR) and its corresponding required measure (*e.g.* the critical ERR). In the context of thermomechanics (Maugin, 1999), this can be referred to as the thermodynamic forces f_k (available to generate damage) being equal to the forces required to generate damage g_k, thus $f_k = g_k$.

The concept of stable damaging processes can be employed within a structural stability formalism where, with the aid of the equality

$f_k = g_k$, a new governing functional, referred to presently as the "extended" total potential energy, can be derived that governs the deformation of a mechanical system and its stability. This is described in detail in the next section.

3. Analytical framework

The current framework employs a discrete coordinate approach in the spirit of the methodology devised by Thompson and Hunt (1973), so that mechanical systems are described by sets of generalized coordinates q_i and loading parameters λ_m. Presently, damage is represented by a set of damage parameters ξ_k such that the total potential energy is given by $\Pi = \Pi(q_i, \lambda_m, \xi_k)$ for a constant state in damage (*i.e.* $\xi_k = \text{const.}$). The total energy of a mechanical system undergoing quasi-static deformation (E) is given by

$$E = \Pi + \Phi \tag{1}$$

where Φ is the dissipative energy associated with K damage processes. In the context of the exposition, it is expedient to assume that the dissipative energy depends on the damage parameters only, even though this is not strictly necessary. The thermodynamic forces available to produce a change in structure (*e.g.* from damage) are given by (*cf.* Maugin, 1999):

$$f_k = -\frac{\partial \Pi}{\partial \xi_k} \tag{2}$$

and their respective critical thresholds (forces required to generate damage) are

$$g_k = \frac{\partial \Phi}{\partial \xi_k}. \tag{3}$$

Employing the necessary condition for stable damage growth, thus

$$f_k(q_i, \lambda_m, \xi_k) = g_k(\xi_k) \tag{4}$$

provides k equations from which relationships for the damage parameters, in terms of $\xi_k = \xi_k(q_i, \lambda_m)$, may be derived if a unique solution is assumed to exist. This assumption holds whenever buckling instability occurs within the elastic range (as considered in the current exposition) and stable damage propagation is present. Closed form expressions may exist for simple application problems (*e.g.* see Schapery, 1987); however, in general, obtaining expressions for ξ_k requires approximation methods, for instance employing a Taylor series expansion (*cf.* Köllner and Völlmecke, 2017a), thus:

$$\begin{aligned}\xi_k = \xi_k^0 &+ \left.\frac{\partial \xi_k}{\partial q_i}\right|_{\substack{q_i^0 \\ \lambda_m^0}} (q_i - q_i^0) + \left.\frac{\partial \xi_k}{\partial \lambda_m}\right|_{\substack{q_i^0 \\ \lambda_m^0}} (\lambda_m - \lambda_m^0) \\ &+ \frac{1}{2}\left.\frac{\partial^2 \xi_k}{\partial q_i \partial q_j}\right|_{\substack{q_i^0 \\ \lambda_m^0}} (q_i - q_i^0)(q_j - q_j^0) \\ &+ \frac{1}{2}\left.\frac{\partial^2 \xi_k}{\partial \lambda_m \partial \lambda_n}\right|_{\substack{q_i^0 \\ \lambda_m^0}} (\lambda_m - \lambda_m^0)(\lambda_n - \lambda_n^0) + \left.\frac{\partial^2 \xi_k}{\partial q_i \partial \lambda_m}\right|_{\substack{q_i^0 \\ \lambda_m^0}} (q_i - q_i^0)(\lambda_m - \lambda_m^0) \\ &+ \mathcal{O}(3),\end{aligned} \tag{5}$$

where partial derivatives of the damage parameters are obtained by implicit differentiation of $D_k[q_i, \lambda_m, \xi_k(q_i, \lambda_m)] = f_k - g_k = 0$ and quantities denoted by $(\bullet)^0$ refer to the current configuration of geometry and loading. As shown in Section 4, a linear approximation of the damage parameters is sufficient in the proposed solution algorithm.

With expressions obtained for the damage parameters ξ_k, a novel energy functional referred to as extended total potential energy Π^* can be derived in which the damage parameters are replaced in the total energy expression (*cf.* Eq. (1)), thus

$$\Pi^* = \Pi^*[q_i, \lambda_m, \xi_k(q_i, \lambda_m)] = \Pi[q_i, \lambda_m, \xi_k(q_i, \lambda_m)] + \Phi[\xi_k(q_i, \lambda_m)]. \tag{6}$$

By replacing the damage parameters, the underlying variational problem in both the configuration and damage state (both would need to be perturbed), *cf.* (Del Piero, 2013), is transformed into a variational principle of the configuration only. As a consequence, the mechanical system is in equilibrium, whenever the first variation of the extended total potential energy vanishes, *i.e.*:

$$\delta\Pi^* = \frac{\partial \Pi^*}{\partial q_i}\delta q_i = 0 \quad \Longrightarrow \quad \frac{\partial \Pi^*}{\partial q_i} = 0. \tag{7}$$

Evaluating the first derivatives of the extended total potential energy results in the following:

$$\frac{\partial \Pi^*}{\partial q_i} = 0 = \underbrace{\frac{\partial \Pi}{\partial q_i}}_{=0} + \underbrace{\left(\frac{\partial \Pi}{\partial \xi_k} + \frac{\partial \Phi}{\partial \xi_k}\right)\frac{\partial \xi_k}{\partial q_i}}_{=0}, \tag{8}$$

where the first term on the right hand side in Eq. (8) is the equilibrium condition and the second term, which can be rewritten as

$$\left(-f_k + g_k\right)\frac{\partial \xi_k}{\partial q_i} = 0, \tag{9}$$

is one of the characteristic conditions governing the damage growth behaviour. It should be noted that in the context of the current exposition, $\partial\xi_k/\partial q_i$ refers to the change in damage from one configuration to another. Enforcing the second law of thermodynamics, *i.e.* healing not being permitted, results in the following condition:

$$\frac{\partial \xi_k}{\partial q_i} \geqslant 0, \tag{10}$$

which constitutes the second condition governing the damage growth behaviour. Thus, Eq. (9) states that either $-f_k + g_k = 0$, which is the necessary condition for stable damage growth, or $\partial\xi_k/\partial q_i = 0$, which requires that $-f_k + g_k > 0$, and consequently introduces the third condition for damage growth, thus

$$-f_k + g_k \geqslant 0. \tag{11}$$

Eq. (11) is considered in the framework by defining each damage parameter in the form of piecewise functions, thus:

$$\xi_k(q_i, \lambda_m) = \begin{cases} \xi_k^0 & \text{if} \quad -f_k + g_k > 0, \\ F_k(q_i, \lambda_m) & \text{if} \quad -f_k + g_k = 0, \end{cases} \tag{12}$$

where functions F_k are either the closed form expressions obtained from Eq. (4) or the approximation as outlined in Eq. (5). It should be noted that ξ_k^0 in Eq. (12) comprises initial measures of the damage parameters (that may also be zero) or constant measures during a deformation process, *i.e.* when a damage parameter changes from being active (growing) to passive (no growth).

Thus, with the extended total potential energy in conjunction with the second law of thermodynamics, alongside a piecewise definition of the damage parameters, the variational principle produces the equilibrium equations (Eq. (7)) and the three conditions required to describe damage growth behaviour (Eqs. (9)–(11)). In the context of the present work, Eqs. (9)–(11) relate to the well-known Kuhn–Tucker conditions for variational problems with (unilateral) constraints.

The stability of an equilibrium state obtained with Eq. (7) can be evaluated by studying higher order variations of the extended total potential energy. Subsequently, the second variation of the extended total potential energy (Π^*) is evaluated, giving:

$$\frac{\partial^2 \Pi^*}{\partial q_i \partial q_j} = \underbrace{\frac{\partial^2 \Pi}{\partial q_i \partial q_j}}_{\lesseqgtr 0 \text{ or } = 0} + \underbrace{\left(-f_k + g_k\right)\frac{\partial^2 \xi_k}{\partial q_i \partial q_j}}_{(A)} + \underbrace{\left(-\frac{\partial f_k}{\partial \xi_l} + \frac{\partial g_k}{\partial \xi_l}\right)\frac{\partial \xi_k}{\partial q_i}\frac{\partial \xi_l}{\partial q_j}}_{(B)}, \tag{13}$$

where relationships in Eqs. (2) and (3) have been substituted. As indicated in Eq. (13), the first term is well-known from the elastic stability formalism (*cf.* Thompson and Hunt, 1973), where positive-definiteness describes stable equilibrium (with zero identifying a bifurcating state

requiring the analysis of higher order variations to evaluate its stability). The term denoted by (A) in Eq. (13) is always zero since during damage growth equality holds between f_k and g_k and whenever $-f_k+g_k>0$, the damage parameters remain unchanged, *i.e.* the second derivatives of the damage parameters are also zero. The final term in Eq. (13), denoted by (B), requires further evaluation. Recall that the first derivative of the damage parameters are always non-negative (*cf.* Eq. (10)). Thus, three possibilities exist in (B):

(I): no damage growth ($\partial\xi_k/\partial q_i = 0$) gives zero,

(II): during growth with $(-\partial f_k/\partial\xi_l + \partial g_k/\partial\xi_l) \geqslant 0$, where a strict inequality describes stable damage propagation and refers to the damage parameter changing from active to passive (*i.e.* growth stops for a constant state of loading) making (B) positive, and the equality indicates a change in stability of the damage mechanisms (*cf.* points of zero slope in Fig. 2(f)) making (B) zero with stability then being determined only by the first term in Eq. (13),

(III): during growth with $(-\partial f_k/\partial\xi_l + \partial g_k/\partial\xi_l) < 0$ makes (B) negative and indicates instability due to unstable damage propagation.

Thus, with the aid of Eq. (13), the stability of equilibrium states can be evaluated, where instability caused by geometry becoming unsuitable (the first term in Eq. (13)) and by unstable damage propagation (the final term in Eq. (13)) can be identified.

Considering the discrete coordinate approach employed, Fig. 3 presents a flowchart for a solution algorithm to determine equilibrium states and evaluate their stability with the present theory. First, for a given mechanical system, the extended total potential energy Π^* is determined, which includes the derivation of the damage parameters, as outlined in Eqs. (4) and (5). For S load steps, the algorithm works as follows. At first, for the current configuration $\{q_i^s, \lambda_m^s, \xi_k^s\}$, the condition $-f_k + g_k$ is evaluated, assigning the current value to the damage parameters if the condition produces a positive output (*i.e.* no damage growth; $\xi_k(q_i,\lambda_m) = \xi_k^s$) or the functions $F_k(q_i,\lambda_m)$ if the condition produces zero (*i.e.* damage growth; $\xi_k(q_i,\lambda_m) = F_k(q_i,\lambda_m)$). Note that a zero output would only be obtained if closed-form expressions for the equilibrium path and for the damage parameters could be determined. In a numerical solution scheme employing approximations of the damage parameters (*cf.* Eq. (5)), as performed in Section 4, a minor numerical error is introduced such that instead of a zero output, marginally negative numbers are obtained, which in fact does not violate the formalism.

In the next step, for the subsequent load step, where Δ_m^s defines the step size for each loading parameter, the equilibrium equations $\partial\Pi^*/\partial q_i = 0$ are solved under the constraint that the change in damage parameters must be non-negative. The stability of the determined equilibrium state $\{q_i^{s+1}, \lambda_m^{s+1}, \xi_k^{s+1}\}$ can then be evaluated with the aid of higher order variations (second order partial derivatives of Π^* are shown in Fig. 3 and described in Eq. (13)). The routine is then repeated for S load steps as necessary.

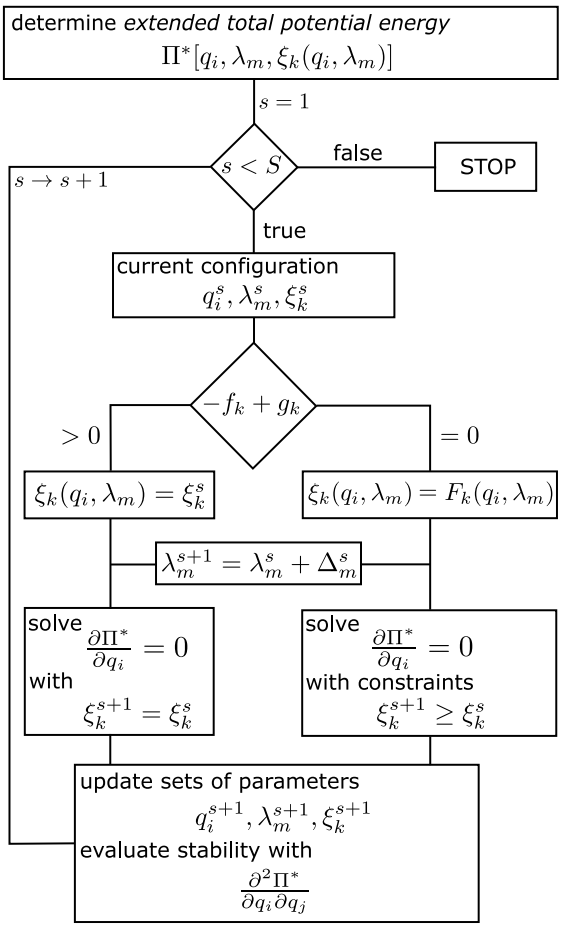


Fig. 3. Solution algorithm flowchart.

4. Application example — composite plate strip with damage

In order to demonstrate the application of the present framework, a one-dimensional model of a carbon fibre reinforced polymer composite panel with multiple types of damage is considered. The problem relates to the common damage type in laminates subject to low-velocity impact scenarios, referred to as barely visible impact damage (BVID); BVID exhibits complex damage morphology comprising multiple delaminations and matrix cracked layers (Baluch et al., 2019; Tuo et al., 2019) and must be considered in the design of aircraft/aerospace structures (European Union Aviation Safety Agency (EASA), 2019). Thus, the mechanical behaviour of such structures under in-plane compressive loading is of particular relevance to the aircraft/aerospace industry (Baker and Murray, 2016). It should be stressed that the application example mainly serves to outline a practical implementation using the new theory. The model does not attempt to capture the complete structural response of composite panels with BVID. Note that (semi-)analytical modelling approaches have, to date, been restricted to assuming stationary damage (Hunt et al., 2004; Köllner et al., 2020; Suemasu, 2016; Sun et al., 2020), the exception being the preliminary work of the authors (Köllner and Völlmecke, 2017a, 2018). Despite employing simplifications such as a one-dimensional problem formulation, the model may, however, be regarded as an initial step towards a semi-analytical description of the compressive response of composite panels with BVID.

4.1. Problem description

Fig. 4 shows the geometric model of a plate strip with two delaminations and matrix cracked layers. The plate strip of length L_{tot} has 28 layers and a $[(0/90)_s]_7$ cross-ply stacking sequence. The delaminations have the length L_1 and L_2, respectively, and their depth is defined by parameters a_1 and a_2. Matrix cracks are assumed to be evenly distributed in the area of the delaminations with a matrix crack density D_{mc} that describes the ratio of the ply thickness to half the distance between two matrix cracks (*cf.* Kashtalyan and Soutis, 2000). Loading is considered in the form of applied compressive strain ε_0.

The model formulation employs the Equivalent Constrained Model, as described in Köllner et al. (2020) and Kashtalyan and Soutis (2000), to determine the in-plane (A_{11}), coupling (B_{11}) and bending (D_{11}) stiffness depending on the matrix crack density D_{mc}, thus $A_{11}(D_{\text{mc}})$, $B_{11}(D_{\text{mc}})$, $D_{11}(D_{\text{mc}})$. Effective stiffness measures, $A_{11}^{\text{eff}}(D_{\text{mc}})$, $B_{11}^{\text{eff}}(D_{\text{mc}})$, $D_{11}^{\text{eff}}(D_{\text{mc}})$, considering coupling effects are determined as outlined in Köllner et al. (2020). The derivation of the stiffness parameters in terms of the matrix crack density is summarized in Appendix A.

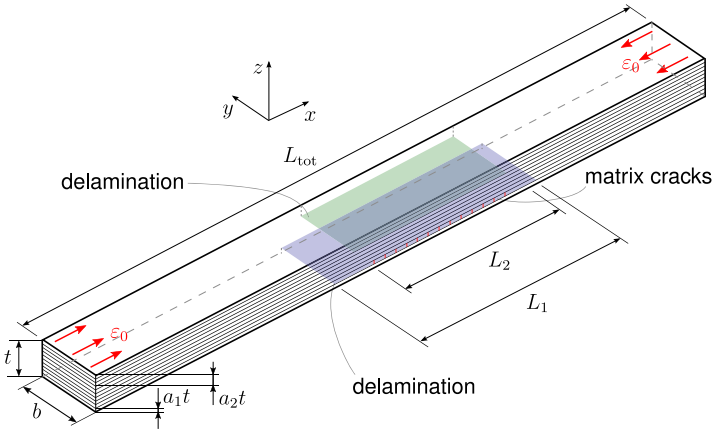


Fig. 4. Geometric model of a plate strip with two delaminations and matrix cracked layers.

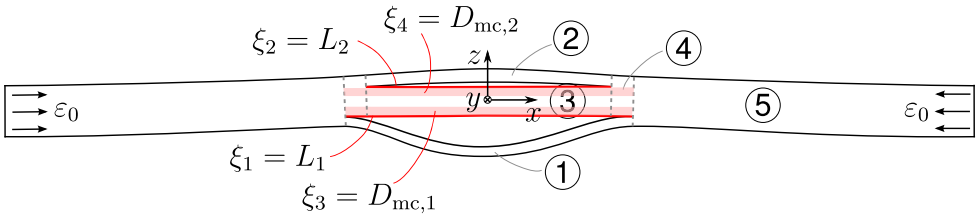


Fig. 5. Sketch of the buckled configuration of the plate strip; two delaminations (ξ_1, ξ_2) and two matrix cracked layers (ξ_3, ξ_4) are depicted.

An additional example demonstrating that the Equivalent Constrained Model can be used to model matrix crack growth adequately for the given problem is provided in Appendix B.

In-plane and out-of-plane displacements, $u(x)$ and $w(x)$ respectively, are approximated by trigonometric series for each part of the plate strip, which are highlighted by circled numbers in Fig. 5. Fig. 5 shows a buckled configuration of the plate strip alongside exemplarily visualizing four damage parameters ($\xi_1, \xi_2, \xi_3, \xi_4$). In the subsequent text, superscript numbers in brackets refer to the respective part of the plate strip, *e.g.* $(\bullet)^{(1)}$ describes a quantity of part ①. Assuming a symmetric buckling response, the out-of-plane displacements of each part are approximated by the buckling expression of the respective Euler case (clamped boundaries at both sides), with the origin of coordinate system being in the middle of the plate strip:

$$
\begin{aligned}
w^{(5)} &= q_5 \cos^2\left(\frac{\pi x}{L_{\text{tot}}}\right), \\
w^{(4)} &= w^{(5)} + q_4 \cos^2\left(\frac{\pi x}{L_1}\right), \quad w^{(3)} = w^{(4)} + q_3 \cos^2\left(\frac{\pi x}{L_2}\right), \\
w^{(2)} &= w^{(4)} + q_2 \cos^2\left(\frac{\pi x}{L_2}\right), \quad w^{(1)} = w^{(5)} + q_1 \cos^2\left(\frac{\pi x}{L_1}\right),
\end{aligned}
\tag{14}
$$

whereas the in-plane displacements are given by:

$$
\begin{aligned}
u^{(5)} &= \varepsilon_0 x + \sum_{n=1}^{N^{(5)}} q_n^{(5)} \sin\left(\frac{2n\pi x}{L_{\text{tot}}}\right), \\
u^{(4)} &= u^{(5)} + \sum_{n=1}^{N^{(4)}} q_n^{(4)} \sin\left(\frac{2n\pi x}{L_1}\right) + \underbrace{z_4 \phi_1 \frac{2x}{L_1}}_{u_4^{\text{rot}}}, \\
u^{(3)} &= \left(u^{(4)} - u_4^{\text{rot}}\right) + \sum_{n=1}^{N^{(3)}} q_n^{(3)} \sin\left(\frac{2n\pi x}{L_2}\right) + z_3 \phi_2 \frac{2x}{L_2}, \\
u^{(2)} &= \left(u^{(4)} - u_4^{\text{rot}}\right) + \sum_{n=1}^{N^{(2)}} q_n^{(2)} \sin\left(\frac{2n\pi x}{L_2}\right) + z_2 \phi_2 \frac{2x}{L_2}, \\
u^{(1)} &= u^{(5)} + \sum_{n=1}^{N^{(1)}} q_n^{(1)} \sin\left(\frac{2n\pi x}{L_1}\right) + z_1 \phi_1 \frac{2x}{L_1}.
\end{aligned}
\tag{15}
$$

In Eq. (15), the parameters z_1, z_2, z_3, z_4 are the offsets between the neutral axis of each part and the parent laminate (part ⑤), and the rotations of the cross-sections (ϕ_1, ϕ_2) are obtained by $\phi_1 = -\partial w^{(5)}/\partial x$ at $x = L_1/2$ and $\phi_2 = -\partial w^{(4)}/\partial x$ at $x = L_2/2$.

With the displacements provided in Eqs. (14) and (15), the axial strain (ε_{xx}) for each part is obtained, thus:

$$
\varepsilon_{xx}^{(n)} = \varepsilon_{xx,0}^{(n)} + z\kappa_{xx}^{(n)} = \frac{\partial u^{(n)}}{\partial x} + \frac{1}{2}\left(\frac{\partial w^{(n)}}{\partial x}\right)^2 + z\left(-\frac{\partial^2 w^{(n)}}{\partial x^2}\right), \tag{16}
$$

where $\varepsilon_{xx,0}^{(n)}$ and $\kappa_{xx}^{(n)}$ are the membrane strain and curvature of the nth part of the plate strip respectively. Note that von Kármán nonlinear strains (second term on the right hand side in Eq. (16)) are considered in order to model nonlinear buckling responses. With Eq. (16), the strain energy (W_{s}) of the plate strip can be determined by $W_{\text{s}} = \sum_{n=1}^{5} W_{\text{s}}^{(n)}$, with:

$$
W_{\text{s}}^{(n)} = \frac{1}{2} b \int_x \left[A_{11}^{\text{eff}(n)} \left(\varepsilon_{xx,0}^{(n)}\right)^2 + 2B_{11}^{\text{eff}(n)} \varepsilon_{xx,0}^{(n)} \kappa_{xx}^{(n)} + D_{11}^{\text{eff}(n)} \left(\kappa_{xx}^{(n)}\right)^2 \right] \mathrm{d}x. \tag{17}
$$

Note that in the displacement-controlled configuration, the total potential energy is the strain energy, *i.e.* $\Pi = W_{\text{s}}$. The application example also requires the consideration of contact between sublaminates (parts ①, ② and ③, as defined in Fig. 5) which may occur during (post-)buckling. Therefore, the constraint conditions $(w^{(2)} - w^{(3)}) \geq 0$ and $(w^{(3)} - w^{(1)}) \geq 0$ are employed by augmenting the strain energy by terms $q_1^{\text{p}}\left[(q_2 - q_3) - \left(c_1^{\text{p}}\right)^2\right]$ and $q_2^{\text{p}}\left[(q_3 - q_1) - \left(c_2^{\text{p}}\right)^2\right]$, where q_p^{p} are Lagrange multipliers representing contact forces and c_p^{p} are offset parameters describing the out-of-plane distance between the sublaminates, which are strictly positive. This represents frictionless hard contact conditions, *cf.* Köllner (2021).

The remaining quantities required for the solution algorithm (*cf.* Fig. 3) are the thermodynamic forces f_k, the dissipative

Table 1
Dimensions and material parameters of the plate strip; material parameters have been taken from Köllner et al. (2021).

Dimensions		Material parameters	
L_{tot}	200 mm	E_{11}	128 GPa
b	10 mm	E_{22}	10.3 GPa
h	0.196 mm	G_{12}	6 GPa
G_{c}^{I}	0.268 N/mm	ν_{12}	0.3

energies associated with the damage mechanisms and the thresholds g_k for producing a change in the structure. For the example provided in Fig. 5, where $K = 4$, the thermodynamic forces are:

$$f_1 = G_1^{\text{del}} = -\frac{1}{b}\frac{\partial W_{\text{s}}}{\partial L_1}, \qquad f_2 = G_2^{\text{del}} = -\frac{1}{b}\frac{\partial W_{\text{s}}}{\partial L_2},$$
$$f_3 = G_1^{\text{mc}} = -\frac{1}{bL_1}\frac{\partial W_{\text{s}}}{\partial D_{\text{mc},1}}, \qquad f_4 = G_2^{\text{mc}} = -\frac{1}{bL_1}\frac{\partial W_{\text{s}}}{\partial D_{\text{mc},2}}, \tag{18}$$

and the associated dissipative energies (in the context of linear elastic fracture mechanics) are

$$\Phi_1 = G_{\text{c}}^{\text{del}} b\left(L_1 - L_1^0\right), \qquad \Phi_2 = G_{\text{c}}^{\text{del}} b\left(L_2 - L_2^0\right),$$
$$\Phi_3 = G_{\text{c}}^{\text{mc}} bL_1\left(D_{\text{mc},1} - D_{\text{mc},1}^0\right), \qquad \Phi_4 = G_{\text{c}}^{\text{mc}} bL_1\left(D_{\text{mc},2} - D_{\text{mc},2}^0\right), \tag{19}$$

resulting in the thresholds g_k (*cf.* Eq. (3)) being $G_{\text{c}}^{\text{del}}$ for the delaminations and G_{c}^{mc} for the matrix cracked layers. Note that quantities denoted by $(\bullet)^0$ refer to initial measures that may also be zero.

Employing the solution algorithm as outlined in Fig. 3, linear approximations of the damage parameters are considered (*cf.* Eq. (5)) making use of Eq. (4) as discussed in Section 3. Linear approximations are acceptable for sufficiently small step sizes during inelastic deformation. With Eqs. (17)–(19) alongside the determined expressions for each damage parameter, the solution algorithm can be implemented, where the extended total potential energy (for the problem visualized in Fig. 5) is given by

$$\Pi^*\left[q_i, \varepsilon_0, \xi_k(q_i, \varepsilon_0)\right] = W_{\text{s}}\left[q_i, \varepsilon_0, \xi_k(q_i, \varepsilon_0)\right] + \Phi\left[\xi_k(q_i, \varepsilon_0)\right] + W_{\text{p}}(q_i, q_p^{\text{p}}, c_p^{\text{p}}). \tag{20}$$

In Eq. (20), $\xi_k = \{L_1(q_i, \varepsilon_0), L_2(q_i, \varepsilon_0), D_{\text{mc},1}(q_i, \varepsilon_0), D_{\text{mc},2}(q_i, \varepsilon_0)\}$, $\Phi = \Phi_1 + \Phi_2 + \Phi_3 + \Phi_4$ and W_{p} is the augmented energy enforcing the contact condition for p contact points. As defined in Eq. (12), it may be noted that all damage parameters are expressed in the form of piecewise functions. All calculations were performed in the software package Mathematica (Wolfram Research, Inc., 2020).

4.2. Results

A cross-ply laminate comprising 28 layers with the stacking sequence $[(0/90)_{\text{s}}]_7$ is studied (the thickness of a layer is denoted by h). The material parameters and dimensions of the plate strip are provided in Table 1. For the approximation of the in-plane displacements, *cf.* Eq. (15), the semi-analytical model employs 24 generalized coordinates with $N^{(5)} = N^{(2)} = N^{(1)} = 6$ and $N^{(3)} = N^{(4)} = 3$, which was found to be sufficient for the configurations studied. Through approximating the out-of-plane displacements as described in Eq. (14), the model comprises only 29 generalized coordinates.

In the current work, two cases of damaged composite plate strips are studied as exemplars to showcase the capabilities of the novel analytical framework. First, the structural response of a plate strip with two delaminations is considered (case 1). This case demonstrates that nonlinear buckling responses in the presence of a single material damaging process can be modelled with the framework. The locations of the two delaminations are close to the top and bottom surface respectively with $a_1 = 1/28$ and $a_2 = 3/28$ (*cf.* Fig. 4). The initial delamination lengths are $L_1 = 39$ mm and $L_2 = 35$ mm, respectively. The results are compared to predictions obtained by finite element (FE) simulations performed in the commercial finite element package ABAQUS (Abaqus, 2019). The FE model is described in detail in Köllner et al. (2020) and uses conventional shell elements (S4R) and employs the virtual crack closure technique (VCCT), *cf.* Krueger (2004). In the semi-analytical and FE model, a mode I fracture criterion is implemented, which is deemed to provide robust conservative, *i.e.* lower bound, predictions due to the one-dimensional description of the problem (direction of growth being predetermined). The critical energy release rate (ERR) is provided in Table 1 (G_{c}^{I}).

For case 1, Fig. 6 shows the structural response in terms of load P versus midpoint deflection w_{mid} (Fig. 6(a)), *i.e.* out-of-plane displacement at the midpoint of part ① (lower sublaminate) and part ② (upper sublaminate), see Fig. 5, alongside load P versus end-shortening $\mathcal{E}$ (Fig. 6(b)).

The structural response obtained by the model (solid black line in Fig. 6) is in excellent agreement with the finite element analysis (FEA, dashed blue line). The nonlinear buckling response within the elastic range, the predictions of the onset of delamination growth (denoted by the symbol "□" in Fig. 6), and the nonlinear buckling response during delamination propagation obtained from the semi-analytical model and the FE simulation practically coincide. The buckling behaviour is characterized by an initial local buckling response of the thinner lower sublaminate (part ①) shown in Fig. 6(a). As applied loading is increased, the thicker sublaminate (part ②) also undergoes local buckling that closes smoothly once global buckling occurs where the parent laminate and the middle part of the plate strip (part ③) deflect in the same direction as the thicker sublaminate (see symbol "•" in Fig. 6). As global buckling progresses, the deflection of the thinner sublaminate shifts to the opposite direction; however, the plate strip remains in an opening mode buckling response (*cf.* Köllner and Völlmecke, 2017b), which is also often referred to as a mixed mode buckling response (*cf.* Hunt et al., 2004; Calvo et al., 2022).

Delamination growth of the lower delamination with length L_1 is generated once global buckling of the plate strip has occurred, which is illustrated in Fig. 6(b) by the decreasing compressive stiffness of the plate strip just prior to reaching the deformation state highlighted by the symbol "□". As can be seen in Fig. 6(a), the increase in delamination length alters the buckling response such that the upper and lower sublaminate deflect in opposite directions during global buckling despite the parent laminate pulling the lower sublaminate into the opposite direction before delamination growth. This response is also verified by the accompanying FE simulation.

Analysing Fig. 6(b), it is noteworthy that the deformation state associated with the initiation of delamination growth ("□" in Fig. 6(b)) constitutes a limit point where further deformation is associated with lower magnitudes of compressive forces, *i.e.* the plate strip cannot withstand the respective compressive force. Thus, in a load-controlled configuration (dead loading), despite undergoing stable deformations within the elastic range, structural instability occurs at the onset of delamination growth, where the system would snap dynamically onto another equilibrium configuration associated with the applied load input or would fail catastrophically. In Fig. 6(b), the plate strip would reach a stable equilibrium state at an end-shortening of approximately 0.9 mm. In contrast, under displacement-controlled loading, the nonlinear buckling response, shown in Fig. 6, is stable even during delamination growth.

Fig. 7 illustrates the delamination propagation of the lower delamination, where the delamination length L_1 is provided against the applied strain ε_0. Additionally, a FE simulation using continuum shell elements (SC8R) is performed, which provides a more precise description of the delamination growth behaviour but requires significantly more computational cost. As can be seen in Fig. 7, all models are in good agreement, where the model using SC8R elements predicts approximately 5% less delamination growth at the maximum applied compressive strain.

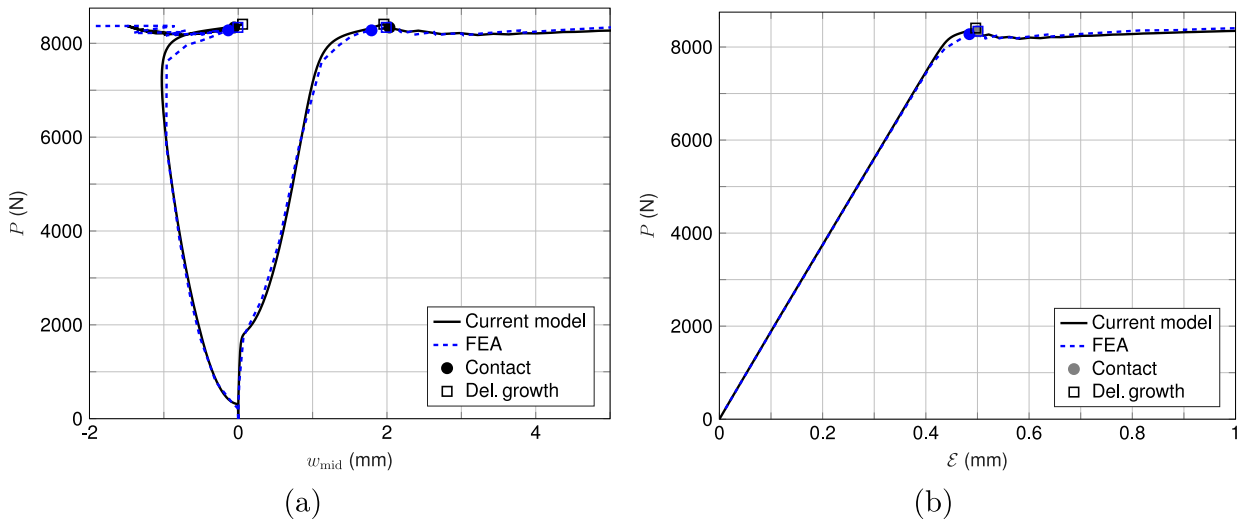


Fig. 6. Nonlinear buckling response – case 1 (two delaminations: $a_1 = 1/28$ and $a_2 = 3/28$ with $L_1 = 39\,\text{mm}$ and $L_2 = 35\,\text{mm}$; no pre-existing matrix cracks); (a) Load P *vs* midpoint deflections w_{mid} of lower sublaminate (part 1 of the plate strip) and upper sublaminate (part 2); (b) Load P *vs* end-shortening $\mathcal{E}$.

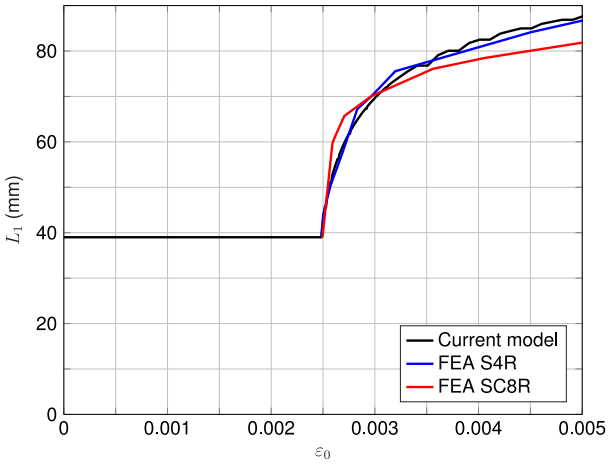


Fig. 7. Delamination growth behaviour in terms of delamination length (L_1) against applied compressive strain (ϵ_0).

The second case studied serves to provide an example for multiple active damage mechanisms and also constitutes an approach towards a more comprehensive representation of damage in a composite plate strip (case 2). Different initial delamination lengths of $L_1 = 98\,\text{mm}$ and $L_2 = 78\,\text{mm}$ are considered while keeping the delamination depth a_1 and a_2 unchanged. In addition, all $(90°)_2$ layers are assumed to exhibit matrix cracks in the form of a matrix crack density D_{mc} (*cf.* Kashtalyan and Soutis, 2000), where exemplarily for all cracked layers D_{mc} is set to 0.1.[1] However, matrix crack densities may also be chosen distinctly and to some extent arbitrarily for each layer. With the matrix cracked layers, the problem formulation considers nine damage mechanisms (two delaminations and seven matrix crack densities).

[1] As shown in Köllner et al. (2020), a matrix crack density of $D_{\text{mc}} = 0.1$ barely affects the stiffness of carbon fibre reinforced unidirectional layers. However, since the application example does not consider the onset of matrix crack formation, introducing matrix cracks enables the evaluation of whether matrix crack growth is caused during nonlinear buckling of the plate strip. Note that no initial matrix cracks are considered in the accompanying FE simulation; however, Hashin's failure criterion (Hashin, 1980) is employed to evaluate whether matrix failure would occur.

For case 2, Fig. 8 shows the structural response in terms of load P versus midpoint deflection w_{mid} (Fig. 8(a)), *i.e.* out-of-plane displacement at the midpoint of part ① and part ②, see Fig. 5, alongside load P versus end-shortening $\mathcal{E}$ (Fig. 8(b)).

In Fig. 8, results of the current semi-analytical model are shown in black solid lines while blue dashed lines are used for the FEA. As in case 1, nonlinear buckling responses before and during damage growth are in very good agreement between the semi-analytical model and the FE simulation. Note that the configuration studied in Fig. 8 causes a different buckling response and has different damage growth characteristics compared to the case presented in Fig. 6. Owing to the larger initial delaminations, the lower (thinner) sublaminate (part ①) and the upper (thicker) sublaminate (part ②) undergo more substantial local buckling responses (see negative and positive midpoint deflection, respectively in Fig. 8(a)) with the middle part (part ③, *cf.* Fig. 5) only undergoing minor out-of-plane deformations due to the shift in neutral axis of the plate strip (*cf.* Simitses et al., 1985). With the onset of global buckling, the middle part (midpoint deflection not shown in Fig. 8(a)) abruptly undergoes buckling deformation where it rather suddenly gets into contact with the thicker lower sublaminate causing a further increase in the buckling resistance of the plate strip. This effect is visualized in Fig. 8(b), where the load versus end-shortening behaviour shows a significant loss in compressive stiffness before contact, denoted by the symbol "•" in Fig. 8, and a subsequent increase in post-buckling stiffness before showing the characteristic weakly stable nonlinear response of a plate strip.

Regarding the structural response during damage growth, Fig. 8 also shows distinct behaviour in comparison with the case studied in Fig. 6. Growth of the lower delamination (L_1), indicated by the symbol "□" in Fig. 8, is initiated without the characteristic drop in load as shown in Fig. 6 and grows stably at first, even if the system would be under load-control. Subsequently, the structure fails abruptly once the second delamination (L_2) starts growing at symbol "⋄" in Fig. 8. At this deformation state, the system loses its stability owing to unstable delamination propagation, where failure is indicated by the vertical dashed line. This response including the initiation of unstable delamination growth is also verified by the FE simulations, where failure is associated with a very slightly smaller load and larger end-shortening.

Note that matrix crack growth is not triggered throughout the deformation process until the initiation of failure at "⋄". This is depicted in Fig. 9 showing the behaviour of the ERR, G, for each damage parameter against applied strain ϵ_0, where, for illustration purposes, ERRs for matrix crack growth are only shown for the four layers exhibiting the largest measures.

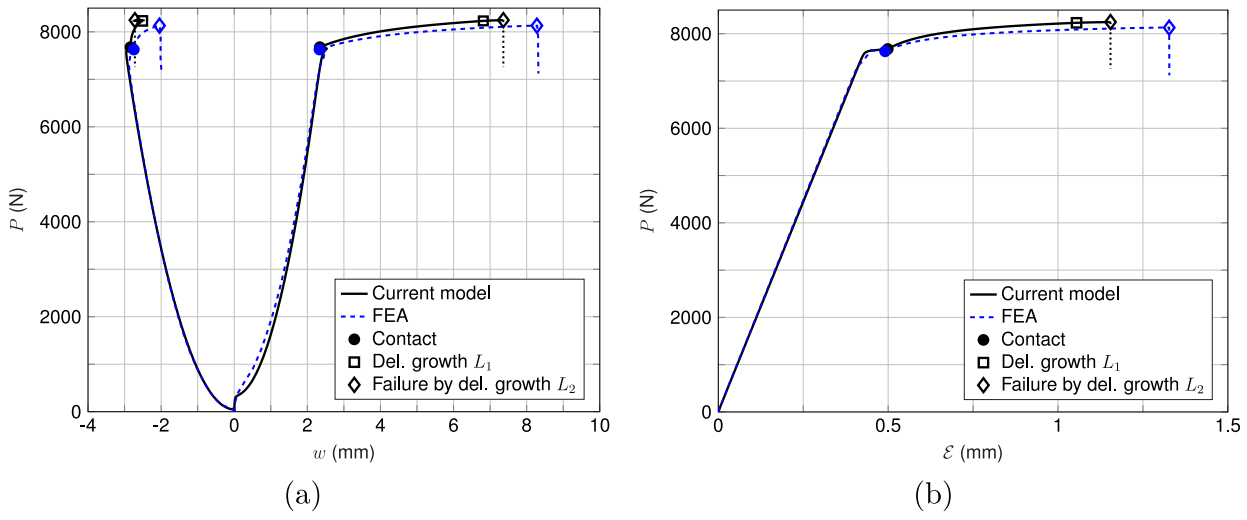


Fig. 8. Nonlinear buckling response – case 2 (two delaminations: $a_1 = 1/28$ and $a_2 = 3/28$ with $L_1 = 98\,\text{mm}$ and $L_2 = 78\,\text{mm}$; all $(90°)_2$ layers with pre-existing matrix cracks $D_{\text{mc}} = 0.1$); (a) Load P *vs* midpoint deflections w_{mid} of lower sublaminate (part 1 of the plate strip) and upper sublaminate (part 2); (b) Load P *vs* end-shortening $\mathcal{E}$.

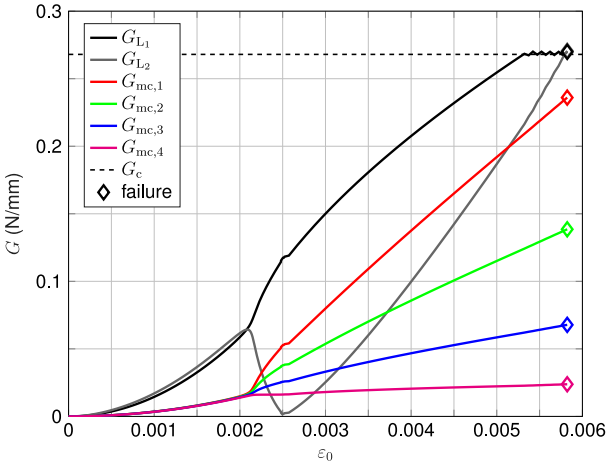


Fig. 9. Energy release rates against applied compressive strain (ε_0) for both delaminations (G_{L}) and matrix cracks (G_{mc}) in four layers.

The initiation of growth of delamination L_1 occurs when G_{L_1} reaches G_{c}. Subsequently, the equality between G_{L_1} and G_{c} holds describing stable damage propagation until delamination L_2 starts to grow; ERRs for matrix crack growth are significantly smaller than for delamination growth except for the most outward layer (*cf.* Köllner et al., 2020), which reaches approximately 90% of the threshold G_{c}.

5. Discussion

The objective of the current work has been the development of an analytical framework such that slender structures undergoing buckling instability which may lead to material damage and its propagation can be efficiently analysed. The framework is embedded into the discrete coordinate approach, as for instance, described by Thompson and Hunt (1973) and considers quasi-static deformation processes, where the novelty of the present work is the extension to deformation processes involving damage and other inelastic effects. Damage is represented by a set of damage parameters, which may also be referred to as internal variables/parameters (Maugin, 1999). The inherent complexity of problems involving buckling instability and material damage is made accessible for (semi-)analytical modelling approaches by exploiting the concept of stable damage growth, where equality holds between thermodynamic forces (damage/crack driving forces) and corresponding thresholds. As a consequence, expressions for damage parameters in terms of the configuration (generalized coordinates) and applied loading can be obtained (at least in an approximative manner), such that damage parameters do not explicitly enter the variational statement. This is different in comparison with variational descriptions of fracture (*cf.* Del Piero, 2013; Bourdin et al., 2008), where both the geometric and damage configuration are perturbed yielding the equilibrium and damage growth conditions. However, in the context of the current work, all three characteristic conditions for describing damage growth (*cf.* Eq. (9)–(11)) can also be obtained by the proposed formalism. This is achieved by the variational principle employing the extended total potential energy alongside enforcing the second law of thermodynamics and defining all damage parameters as piecewise functions. Owing to the *a priori* determination of the expressions for the damage parameters, the solution derived from the variational principle can be very efficiently obtained. This allows a systematic analysis of problems in which structures undergo buckling instability and are vulnerable to material damage.

Assuming explicitly stable damaging processes in the derivation of the framework does not inhibit detecting unstable equilibrium configurations. Instability is characterized by the governing functional, *i.e.* the extended total potential energy, exhibiting a (local) maximum. In contrast, equilibrium paths passing through unstable configurations will not be provided by the framework. However, considering displacement-controlled configurations, instability then constitutes itself in a load–displacement curve by a snap-back response, where unstable equilibrium states are associated with smaller applied strains. Such deformation characteristics may be incorporated *a posteriori* in the framework by either incorporating an arc-length method to trace the equilibrium path, for instance as described in Shen et al. (2021,b) for physical experiments, or an algorithm that finds possible solutions corresponding to the same load input without violating the second law of thermodynamics.

In the matter of evaluating the stability of quasi-static deformation processes involving inelastic deformation, distinctions between the stability of equilibrium configurations and quasi-static processes apply (*cf.* Petryk, 1991). Evaluating the stability of the deformation process rather than equilibrium states is relevant whenever the system undergoes path-dependent deformations. In the context of the current work, implementing the assumption of stable damaging processes implies the introduction of path-independence during damage growth, where the transition from active to passive damaging processes (damage growth to no growth) and *vice versa* is captured by the three conditions governing damage growth (*cf.* Eqs. (9)–(11)). As outlined in Section 3 by

means of analysing the second order variations of the extended total potential energy, the stability of an equilibrium state can be evaluated with the aid of the extended total potential energy where conditions for instability related to geometry and damage can be formulated.

The application of the novel analytical framework has been demonstrated by studying the problem of a composite panel with multiple delaminations and matrix cracked layers loaded under in-plane compression. Structural responses of the plate strip including nonlinear buckling behaviour within the elastic range and during damaging processes have been successfully determined. The responses obtained have been verified by comparison with FE analyses. Various structural (in-)stability phenomena associated with damaging processes have been observed such as stable post-buckling responses during growth, limit point behaviour at the onset of delamination growth, where the plate strip restores to a stable equilibrium configuration at larger deformations, and instability associated with unstable delamination propagation that causes catastrophic failure. The capability of the framework to consider the interplay of multiple damage mechanisms has also been demonstrated.

It should also be stressed that the semi-analytical model does not necessarily have the objective to provide in-depth information about specific damage mechanisms, *i.e.* the approximated displacement field does not as yet offer the capability to consider localizations in the stress/strain field as it occurs around cracks. However, the small number of generalized coordinates, alongside the energy criteria employed, enable a general analysis of the nonlinear structural instability behaviour of damaged composite plate strips and have produced excellent agreement with FE analyses regarding the effect of delamination growth on the overall structural stability.

Thus, apart from providing a blueprint for the application of the analytical framework, the model presented may also be regarded as an initial step towards efficient modelling approaches for the problem of composite panels exhibiting barely visible impact damage loaded under in-plane compression, which is of particular interest to the aircraft industry, where the aforementioned shortcomings would need to be addressed. The required steps towards a more comprehensive description are to extend the model to embedded delaminations (with a 2D problem description, *cf.* Köllner, 2021) and incorporate further damage types, such as fibre breakage as well as geometric imperfections in the form of indentations (Falcó et al., 2022; Lin et al., 2020). It should also be noted that the benefit of describing such systems efficiently may diminish with the increasing requirement of having many generalized coordinates owing to the geometric complexity and for modelling damage mechanisms in greater detail. However, pathways to transfer the analytical formalism into a finite element framework (*cf.* Pineda and Waas, 2013) appear to be feasible and will be explored next.

6. Concluding remarks

A novel analytical framework for a structural stability analysis of mechanical systems vulnerable to buckling instability and material damage has been presented. The work addresses the need for efficient analysis tools in current engineering practice where, owing to modern materials (composite materials/structures) and the pursuit of more sustainable engineering solutions, the design of engineering structures requires either the explicit consideration of damage (*e.g.* damage tolerant design) and/or the full exploitation of structural strength. As a consequence, structures prone to buckling instability must inevitably also consider material damage and plasticity. However, modelling such deformation processes normally relies solely on high-fidelity numerical approaches that often turn out to be unfeasible for design practice regarding associated computational costs (*e.g.* for determining the compressive strength of composite structures with BVID). On the other hand, where simpler materials and structures still enable efficient designs (*e.g.* steel structural members in civil engineering applications), design recommendations are often based largely on empiricism that may impede the full understanding and hence utilization of the structural load carrying capacity.

In order to resolve this issue, the current work has presented a framework where the concept of stable damage growth is incorporated within a structural stability analysis formalism. The framework allows efficient (semi-)analytical models to be developed that employ a so-called extended total potential energy in which damage parameters are expressed in terms of the structural configuration and applied loading. The derived variational principle employing the extended total potential energy in conjunction with the second law of thermodynamics and a piecewise definition of damage parameters provides the equilibrium conditions alongside the required conditions to describe damage growth. Higher order variations of the extended total potential energy determine the stability of equilibrium states.

In its current form, the framework considers mechanical systems that are described by sets of generalized coordinates, loading parameters and damage parameters, undergoing quasi-static deformation processes. The application of the framework has been demonstrated by studying the compressive response of composite panels with multiple delaminations and matrix cracked layers. Nonlinear buckling responses have been obtained for characteristic configurations causing distinct structural instability phenomena associated with delamination growth providing the foundation for a general structural stability analysis of damaged composite panels. Further characteristic application examples range from composite panels with BVID to structural members used in civil engineering construction.

CRediT authorship contribution statement

Anton Köllner: Conceptualization, Methodology, Investigation, Data curation, Formal analysis, Software, Funding acquisition, Writing – original draft, Writing – review & editing. **M. Ahmer Wadee:** Investigation, Funding acquisition, Project administration, Writing – review & editing.

Declaration of competing interest

The authors declare that they have no known competing financial interests or personal relationships that could have appeared to influence the work reported in this paper.

Data availability

Data will be made available on request.

Acknowledgements

This project has received funding from the European Union's Horizon 2020 research and innovation programme under the Marie Skłodowska-Curie grant agreement No 842543 (project title: "DamBuckler").

Appendix A. Equivalent constrained model

The derivation of the reduced in-plane stiffness matrix due to matrix cracks by employing the Equivalent Constrained Model is briefly summarized and follows information provided in Köllner et al. (2020). A detailed derivation can be found in Kashtalyan and Soutis (2000, 2016) and Zhang et al. (1992).

Considering a cross-ply laminate that exhibits matrix cracks in a 90° layer, as used in Section 4.1, the actual cracked layer can be replaced by an equivalent homogeneous layer possessing degraded stiffness properties. The reduced in-plane stiffness matrix of the equivalent

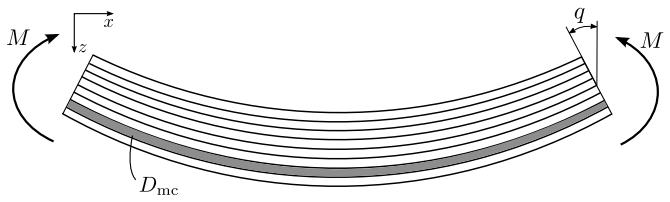


Fig. B.1. Geometric model of a $(0/90)_{2s}$ laminate subjected to a uniform bending moment M.

homogeneous layer $[\bar{Q}^{(90)}]$ (in the local coordinate system of the 90° layer) is expressed as follows:

$$[\bar{Q}^{(90)}] = [\hat{Q}^{(90)}] - \begin{bmatrix} \frac{\left(\hat{Q}_{12}^{(90)}\right)^2}{\hat{Q}_{22}^{(90)}} \Lambda_{22}^{(90)} & \hat{Q}_{12}^{(90)} \Lambda_{22}^{(90)} & 0 \\ \hat{Q}_{12}^{(90)} \Lambda_{22}^{(90)} & \hat{Q}_{22}^{(90)} \Lambda_{22}^{(90)} & 0 \\ 0 & 0 & \hat{Q}_{66}^{(90)} \Lambda_{66}^{(90)} \end{bmatrix}, \tag{A.1}$$

where $[\hat{Q}^{(90)}]$ is the in-plane stiffness matrix of the undamaged layer and $\Lambda_{22}^{(90)}$ and $\Lambda_{66}^{(90)}$ are 'In-situ Damage Effective Functions', see Zhang et al. (1992).

The In-situ Damage Effective Functions $(\Lambda_{22}^{(90)}, \Lambda_{66}^{(90)})$ are explicit functions of the relative transverse crack density D_{mc}, defined as the thickness of the layer divided by half the distance in between two matrix cracks, and can be obtained in closed form thus:

$$\Lambda_{22}^{(90)} = \frac{1 - \frac{D_{mc}}{\beta_1^{(90)}} \tanh\left(\frac{\beta_1^{(90)}}{D_{mc}}\right)}{1 + \alpha_1^{(90)} \frac{D_{mc}}{\beta_1^{(90)}} \tanh\left(\frac{\beta_1^{(90)}}{D_{mc}}\right)} \quad \text{and}$$

$$\Lambda_{66}^{(90)} = \frac{1 - \frac{D_{mc}}{\beta_2^{(90)}} \tanh\left(\frac{\beta_2^{(90)}}{D_{mc}}\right)}{1 + \alpha_2^{(90)} \frac{D_{mc}}{\beta_2^{(90)}} \tanh\left(\frac{\beta_2^{(90)}}{D_{mc}}\right)}, \tag{A.2}$$

where the constants $\beta_1^{(90)}$, $\beta_2^{(90)}$, $\alpha_1^{(90)}$ and $\alpha_2^{(90)}$ are provided in Köllner et al. (2020) and Kashtalyan and Soutis (2000) and depend solely on the compliances of the undamaged 0° and 90° layers respectively, in-plane stiffnesses of the undamaged 90° layer, shear lag parameters and a layer thickness ratio.

The reduced stiffness matrix provided in Eq. (A.1) is employed in the current model to determine in-plane, coupling and bending stiffnesses of the plate strip and the sublaminates, respectively, as outlined in Section 4.1.

Appendix B. Cross-ply laminate under flexure – matrix crack growth

In order to demonstrate the modelling of progressive matrix crack growth using the Equivalent Constraint Model in the context of the application example provided in Section 4, the problem of a cross-ply laminate under pure bending is exemplarily considered. The problem description follows Smith and Ogin (2000), where an eight layer $(0/90)_{2s}$ laminate is studied in a four point bending test. The corresponding geometric model for the cross-ply laminate subjected to a bending moment M is shown in Fig. B.1.

Matrix crack growth for the most outward 90° layer (on the side subjected to tension) is studied, which is highlighted in grey in Fig. B.1, where the corresponding matrix crack density is denoted by D_{mc}. The problem is described by means of a single degree of freedom (DOF) which is the rotation of the cross-section where the bending moment is applied. The corresponding generalized coordinate q is visualized in Fig. B.1. If deemed necessary, more generalized coordinates may, of course, be employed which also applies to considering out-of-plane shear deformation as well as residual (thermal) strains (as done in Smith and Ogin, 2000). However, presently the focus is solely on demonstrating that modelling matrix crack growth using the Equivalent Constrained Model is feasible for the problem studied within the current work.

Table B.1
Dimensions and material parameters of the cross-ply laminate; taken from Smith and Ogin (2000).

Dimensions		Material parameters	
L	77 mm	E_{11}	37 GPa
b	20 mm	E_{22}	9.5 GPa
h	0.5 mm	G_{12}	4 GPa
G_c^{mc}	0.246 N/mm	ν_{12}	0.28

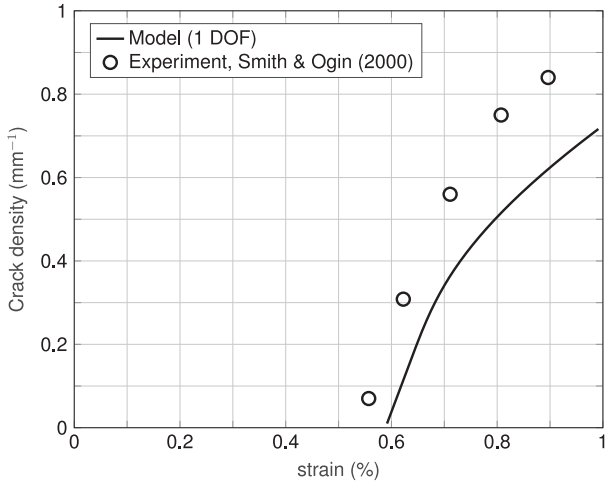


Fig. B.2. Matrix crack density against axial strain in the 90° layer.

The extended total potential energy of the system is given by

$$\Pi^* = \frac{1}{2} b D_{11} \int_L \left(\kappa_{xx}\right)^2 \, \mathrm{d}x + G_c^{mc} b L \left[D_{mc}(q, M) - D_{mc}^0\right] - 2Mq, \tag{B.1}$$

where the bending stiffness D_{11} depends on the matrix crack density D_{mc} which is expressed in the form of $D_{mc}(q, M)$ using the analytical framework provided in Section 3. The bending stiffness D_{11} is calculated employing the Equivalent Constrained Model expressing the in-plane reduced stiffness matrix of the most outward 90° layer (*cf.* Fig. B.1) by Eq. (A.1) while making use of Eq. (A.2).

Note that the damage parameter D_{mc} is expressed as a piecewise function, as shown in Eq. (12). In Eq. (B.1), linearized curvatures are considered ($\kappa_{xx} \approx -\partial^2 w / \partial x^2$), with the length and the width of the laminate being denoted as L and b respectively. The out-of-plane displacement is approximated by $w = qx(L - x)/L$. The critical energy release rate is denoted by G_c^{mc}. The dimensions and material parameters of the laminate are taken from Smith and Ogin (2000) and are provided in Table B.1.

By employing the solution algorithm outlined in Section 3, the deformation behaviour of the laminate under bending can be obtained considering possible matrix crack growth. With the Equivalent Constrained Model implemented, a negligibly small initial matrix crack density D_{mc}^0 must be assumed to be present in the respective layer to avoid numerical singularities (see Eq. (A.2)). In the subsequent analysis, this measure is set to 0.01. The results obtained by the simple 1-DOF model are compared against experimental findings documented in Smith and Ogin (2000). In Fig. B.2, the behaviour of the matrix crack density against the axial strain in the respective 90° layer is visualized. Note that to obtain the measure of crack density used in Smith and Ogin (2000), the crack density $D_{mc} = h^{(90)}/s$ needs to be multiplied by $1/2h^{(90)}$.

Matrix crack growth is initiated at a strain of approximately 0.58%. A significant increase in crack density (high rate of crack growth) can

be observed following crack growth initiation. In between crack densities of 0.3–0.4 mm^{-1}, the rate of crack growth slows which appears to proceed for increasing strains. The predictions of the 1-DOF model are in good agreement with experimental findings for crack densities of up to 0.4 mm^{-1}, where subsequently the deviations between model and experimental observations increase; however, the qualitative behaviour of a decreasing rate of crack growth is also shown in the experiments. Predictions for higher crack densities may of course be improved by considering out-of-plane shear deformations in conjunction with employing more DOFs.

In summary, with the aid of the simple 1-DOF model in conjunction with comparisons to experimental findings, it has been shown that matrix crack growth (whenever initiated) can be adequately modelled using the Equivalent Constrained Model in the context of the application example provided in Section 4.

References

Abambres, M., Camotim, D., Silvestre, N., Rasmussen, K.J.R., 2014. GBT-based structural analysis of elastic–plastic thin-walled members. Comp. Struct. 136, 1–23.

Abaqus, 2019. ABAQUS/Standard. Dassault Systèmes, Providence RI, USA.

Bai, L., Wadee, M.A., Köllner, A., Yang, J., 2021. Variational modelling of local–global mode interaction in long rectangular hollow section struts with Ramberg–Osgood type material nonlinearity. Int. J. Mech. Sci. 209, 106691.

Baker, A.A., Murray, L.S., 2016. Composite Materials for Aircraft Structures. AIAA Education Series.

Baluch, A.H., Falcó, O., Jiménez, J.L., Tijs, B.H.A.H., Lopes, C.S., 2019. An efficient numerical approach to the prediction of laminate tolerance to barely visible impact damage. Compos. Struct. 225, 111017.

Bažant, Z.P., Cedolin, L., 2010. Stability of Structures: Elastic, Inelastic, Fracture and Damage Theories. World Scientific.

Bigoni, D., 2000. Bifurcation and instability of non-associative elastoplastic solids. In: Petryk, H. (Ed.), Material Instabilities in Elastic and Plastic Solids. In: CISM Lecture Notes, vol. 414, Springer, pp. 1–52.

Bordignon, A., Piccolroaz, A., Dal Corso, F., Bigoni, D., 2015. Strain localization and shear banding in ductile materials. Front. Mater. 2, 1–13.

Bourdin, B., Francfort, G.A., Marigo, J.J., 2008. The variational approach to fracture. J. Elasticity 91, 5–148.

Calvo, J.V., Feito, N., Miguélez, M.H., Giner, E., 2022. Modeling the delamination failure under compressive loads in CFRP laminates based on digital image correlation analysis. Compos. Struct. 287, 115265.

Del Piero, G., 2013. A variational approach to fracture and other inelastic phenomena. J. Elast. 112 (1), 3–77.

European Union Aviation Safety Agency (EASA), 2019. AMC 20-29 effective: 26/07/2010. URL: https://www.easa.europa.eu/sites/default/files/dfu/Annex%20II%20-%20AMC%2020-29.pdf.

Falcó, O., Lopes, C.S., Sommer, D.E., Thomson, D., Ávila, R.L., Tijs, B.H.A.H., 2022. Experimental analysis and simulation of low-velocity impact damage of composite laminates. Compos. Struct. 287, 115278.

Francfort, G.A., Marigo, J.-J., 1998. Revisiting brittle fracture as an energy minimization problem. J. Mech. Phys. Solids 46 (8), 1319–1342.

Gardner, L., 2008. The continuous strength method. Proc. Inst. Civ. Eng.: Struct. Build. 161 (3), 127–133.

Gardner, L., 2019. Stability and design of stainless steel structures – Review and outlook. Thin-Walled Struct. 141, 208–216.

Gonçalves, R., Camotim, D., 2012. Geometrically non-linear generalised beam theory for elastoplastic thin-walled metal members. Thin-Walled Struct. 51, 121–129.

Hashin, Z., 1980. Failure criteria for unidirectional fiber composites. J. Appl. Mech. 47 (2), 329–334.

Hill, R., 1958. A general theory of uniqueness and stability in elastic-plastic solids. J. Mech. Phys. Solids 6, 236–246.

Hill, R., 1962. Uniqueness criteria and extremum principles in self-adjoint problems of continuum mechanics. J. Mech. Phys. Solids 10, 185–194.

Hunt, G.W., Hu, B., Butler, R., Almond, D.P., Wright, J.E., 2004. Nonlinear modeling of delaminated struts. AIAA J. 42 (11), 2364–2372.

Hutchinson, J.W., 1974. Plastic buckling. Adv. Appl. Mech. 14, 67–144.

Juhász, Z., Szekrényes, A., 2015. Progressive buckling of a simply supported delaminated orthotropic rectangular composite plate. Int. J. Solids Struct. 69–70, 217–229.

Juhász, Z., Szekrényes, A., 2017. The effect of delamination on the critical buckling force of composite plates: Experiment and simulation. Compos. Struct. 168, 456–464.

Kashtalyan, M., Soutis, C., 2000. Stiffness degradation in cross-ply laminates damaged by transverse cracking and splitting. Composites A 31 (4), 335–351.

Kashtalyan, M., Soutis, C., 2016. Modelling of stiffness degradation due to cracking in laminates subjected to multi-axial loading. Phil. Trans. R. Soc. A 374 (20–21), 20160017.

Koiter, W.T., 1945. On the Stability of Elastic Equilibrium (Ph.D. thesis). Technische Hogeschool, Delft (Technological University of Delft), The Netherlands. English translation issued as NASA, *Tech. Trans.*, F 10, 833.

Köllner, A., 2021. Predicting buckling-driven delamination propagation in composite laminates: An analytical modelling approach. Compos. Struct. 266, 113776.

Köllner, A., Kashtalyan, M., Guz, I., Völlmecke, C., 2020. On the interaction of delamination buckling and damage growth in cross-ply laminates. Int. J. Solids Struct. 120–121, 912–928.

Köllner, A., Nielsen, M.W.D., Srisuriyachot, J., Rhead, A.T., Butler, R., 2021. Buckle-driven delamination models for laminate strength prediction and damage tolerant design. Thin-Walled Struct. 161, 107468.

Köllner, A., Völlmecke, C., 2017a. An analytical framework to extend the general structural stability analysis by considering certain inelastic effects—theory and application to delaminated composites. Compos. Struct. 170, 261–270.

Köllner, A., Völlmecke, C., 2017b. Buckling and postbuckling behaviour of delaminated composite struts. Int. J. Comput. Methods Eng. Sci. Mech. 18 (1), 25–33.

Köllner, A., Völlmecke, C., 2018. Post-buckling behaviour and delamination growth characteristics of delaminated composite plates. Compos. Struct. 203, 777–788.

Krueger, R., 2004. Virtual crack closure technique: History, approach, and applications. Appl. Mech. Rev. 57 (2), 109–143.

Lin, S., Thorsson, S.I., Waas, A.M., 2020. Predicting the low velocity impact damage of a quasi-isotropic laminate using EST. Compos. Struct. 112530.

Liu, B., Xu, F., Qin, J., Lu, Z., 2017. Study on impact damage mechanisms and TAI capacity for the composite scarf repair of the primary load-bearing level. Compos. Struct. 181, 183–193.

Maugin, G.A., 1999. The Thermomechanics of Nonlinear Irreversible Behaviors. World Scientific.

Nettles, A.T., Douglas, M.J., 2000. A Comparison of Quasi-Static Indentation Testing to Low Velocity Impact Testing, Composite Materials: testing, Design and Acceptance Criteria. Standard. American Society for Testing and Materials.

Petryk, H., 1991. The energy criteria of instability in time-independent inelastic solids. Arch. Mech. 43 (4), 519–545.

Petryk, H., 2005. Thermodynamic conditions for stability in materials with independent dissipation. Phil. Trans. R. Soc. A 363, 2479–2515.

Petryk, H., Thermann, K., 1992. On discretized plasticity problems with bifurcations. Int. J. Solids Struct. 29 (6), 745–765.

Pineda, E.J., Waas, A.M., 2013. Numerical implementation of a multiple-ISV thermodynamically-based work potential theory for modeling progressive damage and failure in fiber-reinforced laminates. Int. J. Fract. 182, 93–122.

Schapery, R.A., 1987. Deformation and fracture characterization of inelastic composite materials using potentials. Polym. Eng. Sci. 27 (1), 63–76.

Schapery, R.A., 1990. A theory of mechanical behavior of elastic media with growing damage other changes in structure. J. Mech. Phys. Solids 38 (2), 215–253.

Shen, J., Groh, R.M.J., Schenk, M., Pirrera, A., 2021. Experimental path-following of equilibria using Newton's method. Part I: Theory, modelling, experiments. Int. J. Solids Struct. 210, 203–223.

Shen, J., Groh, R.M.J., Schenk, M., Pirrera, A., 2021b. Experimental path-following of equilibria using Newton's method. Part II: Applications and outlook. Int. J. Solids Struct. 213, 25–40.

Simitses, G.J., Sallam, S., Yin, W.L., 1985. Effect of delamination of axially loaded Homogeneous laminated plates. AIAA J. 23 (9), 1437–1444.

Smith, P.A., Ogin, S.L., 2000. Characterization and modelling of matrix cracking in a $(0/90)_{2s}$ GFRP laminate loaded in flexure. Proc. R. Soc. Lond. Ser. A Math. Phys. Eng. Sci. 456, 2755–2770.

Suemasu, H., 2016. Analytical approaches to compression after impact (CAI) behavior of carbon fiber-reinforced composite materials. Adv. Compos. Mater. 25 (1), 1–18.

Sumi, Y., Nemat-Nasser, S., Keer, L.M., 1985. On crack path stability in a finite body. Eng. Fract. Mech. 22 (5), 759–771.

Sun, X.C., Hallett, S.R., 2018. Failure mechanisms and damage evolution of laminated composites under compression after impact (CAI): Experimental and numerical study. Composites A 104, 41–59.

Sun, X.C., Hallett, S.R., Suemasu, H., Wisnom, M.R., 2020. Simplified analytical approximations for scaled composite laminates under transverse loading. Compos. Struct. 236, 111745.

Tan, W., Falzon, B.G., Chiu, L.N.S., Price, M., 2016. Predicting low velocity impact damage and compression-after-impact(CAI) behaviour of composite laminates. Composites A 71, 212–226.

Thompson, J.M.T., Hunt, G.W., 1973. A General Theory of Elastic Stability. John Wiley & Sons.

Tuo, H., Lu, Z., Ma, X., Xing, J., Zhang, C., 2019. Damage and failure mechanism of thin composite laminates under low-velocity impact and compression-after-impact loading conditions. Composites B 163, 642–654.

Tvergaard, V., 1983. Plastic buckling of axially compressed circular cylindrical shells. Thin-Walled Struct. 1, 139–163.

Wadee, M.A., 2002. Localized buckling in sandwich struts with pre-existing delaminations and geometrical imperfections. J. Mech. Phys. Solids 50, 1767–1787.
Wadee, M.A., Blackmore, A., 2001. Delamination from localized instabilities in compression sandwich panels. J. Mech. Phys. Solids 49, 1281–1299.
Wang, K., Zhao, L., Hong, H., Zhang, J., Hu, N., 2020. An extended analytical model for predicting the compressive failure behaviors of composite laminate with an arbitrary elliptical delamination. Int. J. Solids Struct. 185–186, 439–447.
Wolfram Research, Inc., 2020. Mathematica, Version 12.0. Champaign, IL.
Zhang, J., Fan, J., Soutis, C., 1992. Analysis of multiple matrix cracking in composite laminates part 1: In-plane stiffness properties. Composites 23 (5), 291–298.